Full parity phase diagram of a proximitized nanowire island

Shen, J.; Winkler, G. W.; Borsoi, F.; Heedt, S.; Levajac, V.; Wang, J. Y.; van Driel, D.; Bouman, D.; Kouwenhoven, L. P.; van Heck, B.

DOI
10.1103/PhysRevB.104.045422

Publication date
2021

Document Version
Final published version

Published in
Physical Review B

Full parity phase diagram of a proximitized nanowire island

J. Shen [1,2,*] G. W. Winkler [3] F. Borsoi [1] S. Heedt [1,4] V. Levajac,[1] J.-Y. Wang,[1] D. van Driel,[1] D. Bouman [1] S. Gazibegovic,[5] R. L. M. Op Het Veld,[5] D. Car,[5] J. A. Logan [6] M. Pendharkar [7] C. J. Palmstrøm,[6,7] E. P. A. M. Bakkers,[5] L. P. Kouwenhoven,[1,4] and B. van Heck [4,†]

[1]*QuTech and Kavli Institute of Nanoscience, Delft University of Technology, 2600 GA Delft, The Netherlands*
[2]*Beijing National Laboratory for Condensed Matter Physics, Institute of Physics, Chinese Academy of Sciences, Beijing 100190, China*
[3]*Microsoft Quantum, Microsoft Station Q, University of California Santa Barbara, Santa Barbara, California 93106, USA*
[4]*Microsoft Quantum Lab Delft, 2600 GA Delft, The Netherlands*
[5]*Department of Applied Physics, Eindhoven University of Technology, 5600 MB Eindhoven, The Netherlands*
[6]*Materials Department, University of California Santa Barbara, Santa Barbara, California 93106, USA*
[7]*Electrical and Computer Engineering, University of California Santa Barbara, Santa Barbara, California 93106, USA*

(Received 18 December 2020; revised 12 April 2021; accepted 7 July 2021; published 21 July 2021)

We measure the charge periodicity of Coulomb blockade conductance oscillations of a hybrid InSb-Al island as a function of gate voltage and parallel magnetic field. The periodicity changes from $2e$ to $1e$ at a gate-dependent value of the magnetic field, B^*, decreasing from a high to a low limit upon increasing the gate voltage. In the gate voltage region between the two limits, which our numerical simulations indicate to be the most promising for locating Majorana zero modes, we observe correlated oscillations of peak spacings and heights. For positive gate voltages, the $2e$-$1e$ transition with low B^* is due to the presence of nontopological states whose energy quickly disperses below the charging energy due to the orbital effect of the magnetic field. Our measurements highlight the importance of a careful exploration of the entire available phase space of a proximitized nanowire as a prerequisite to define future topological qubits.

DOI: 10.1103/PhysRevB.104.045422

I. INTRODUCTION

Coulomb blockade conductance oscillations provide quantitative information about the charge and energy spectrum of a mesoscopic island [1]. The charge periodicity of the oscillations can be directly related to the free-energy difference between even and odd fermion parity states of the island [2]. In superconducting islands, the periodicity is $2e$ [2–5], reflecting the presence of a superconducting ground state with even fermion parity. In gate-defined semiconducting dots, on the other hand, the periodicity is $1e$, up to peak-to-peak variations due the individual energy levels of the dot [6–8].

Hybrid semiconducting-superconducting islands can be tuned to exhibit both periodicities [9–20]. In particular, a magnetic field can be used to tune the periodicity from $2e$ to $1e$, with an intermediate "even-odd" regime characterized by a bimodal distribution of peak spacings [10]. This change in periodicity can be associated with the exciting possibility of a transition into a topological phase with Majorana zero modes [21–23], with potential applications in topological quantum computing [24,25]. The $2e$-to-$1e$ transition, however, is a necessary but not sufficient condition to determine the presence of a topological phase [26], since it can be caused by any Andreev bound state [27–29] whose energy decreases below the charging energy of the island. In fact, early experimental findings on InAs-Al and InSb-Al islands (e.g., Refs. [10–13]) are not fully consistent with a Majorana interpretation. Possible discrepancies are the decreasing amplitude of even-odd peak spacing oscillations with magnetic field [30–33], as well as the low field at which $1e$ periodicity appeared, compared to the expected value for the topological transition to occur.

In this paper, we report an exhaustive measurement of the Coulomb oscillations in an InSb-Al island as a function of gate voltage and magnetic field. Our goal is to map out the entire measurable phase space of the island in order to identify potential topological regions and compare their locations to the expected topological phase diagram resulting from state-of-the-art numerical simulations. We find that the $2e$-to-$1e$ transition happens at a value of the magnetic field, B^*, which decreases with increasing gate voltage in agreement with simulations. Regions with a very low B^* are unlikely to be topological, while the most promising gate range occurs at intermediate values of B^*.

II. MEASUREMENT OF THE PARITY PHASE DIAGRAM

The experiment is carried out in the device shown in Fig. 1. It consists of a hybrid InSb-Al nanowire [34], in which two crystallographic facets of the hexagonal InSb cross section are covered by 8–15 nm of epitaxial Al film. The length of the proximitized segment of the nanowire is ≈ 1 μm. The nanowire is contacted with metallic source and drain leads, and coupled to three gates for electrostatic control. The two gates on the sides act as tunnel gates, while the middle gate acts as a plunger gate controlling the electron occupation of the island as well as the cross-sectional profile of the electron

*shenjie@iphy.ac.cn
†bernard.vanheck@microsoft.com

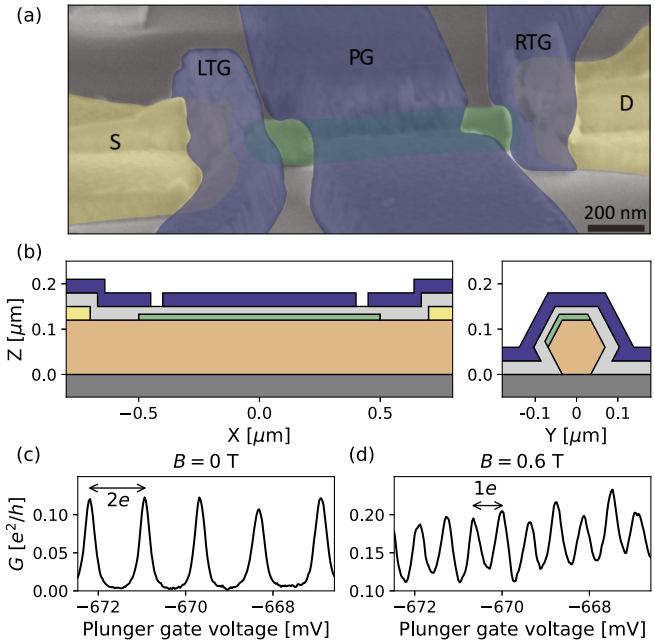

FIG. 1. (a) Scanning electron microscopy image of the experimental device with false colors. Labels indicate source (S), drain (D), left and right tunnel gates (LTG, RTG), and plunger gate (PG). The Al shell is colored in green. (b) Longitudinal (left) and cross-sectional (right) cuts of the model used in the simulations: substrate (dark gray), InSb nanowire (orange), Al (green), Ohmic contacts (yellow), dielectric (gray), and gates (blue). Conductance oscillations measured at zero bias voltage exhibit $2e$ peak spacings at $B = 0$ (c) and $1e$ peak spacings at $B = 0.6$ T (d).

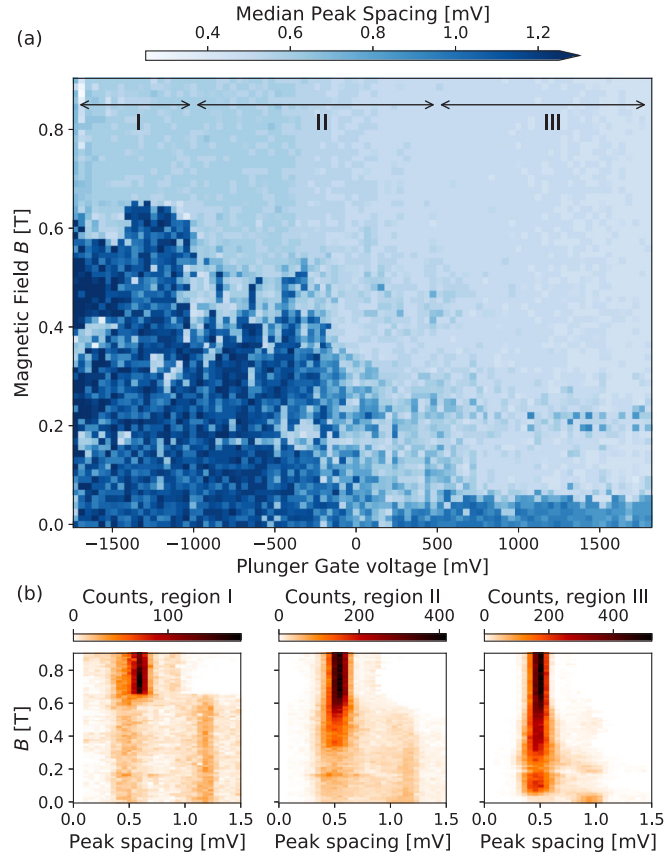

FIG. 2. (a) Median peak spacing of Coulomb blockade oscillations as a function of magnetic field and gate voltage. Dark-blue areas correspond to predominant $2e$ periodicity, and light blue to $1e$ periodicity. For each pixel, the median is determined from a window of 20 mV in plunger gate voltage, corresponding to ≈20–40 conductance oscillations. (b) Peak spacing distributions for regions I, II, and III as labeled in panel (a). We attribute the presence of a residual $1e$ peak at low B in region I to the possible poisoning of the island [11] as well as to the occasional presence of subgap states [13].

density in the semiconductor. A magnetic field B, parallel to the nanowire axis, can be applied to the device.

The device under consideration shows a hard superconducting gap [34] as well as $2e$-periodic Coulomb oscillations at $B = 0$ [13]. An example of the latter is shown in Fig. 1(c), with a $2e$ peak spacing ≈1.2 mV. From the measurement of the $2e$-periodic Coulomb diamonds [35], we extract a single-electron charging energy $E_C = e^2/2C \approx 40$ μeV for the island. In a large magnetic field, the Coulomb oscillations become $1e$ periodic, as shown in Fig. 1(d).

The magnetic field B^* at which the periodicity changes from $2e$ to $1e$ depends on the plunger gate voltage. To determine this, we have measured a sequence of 90 conductance traces for each magnetic field, centered 40 mV apart in the plunger gate and covering a total range of 3.6 V in the plunger gate as well as 0.9 T in magnetic field. Each trace spans 20 mV and contains a sequence of 20–40 Coulomb blockade oscillations from which we extract the peak spacings [35]. A telling picture emerges when plotting the median of the peak spacing distribution at each point in parameter space [Fig. 2(a)]. This experimental phase diagram can be heuristically divided into three plunger gate voltage regions, which we denote regions I, II, and III going from negative to positive gate voltages.

In region I, the $2e$-to-$1e$ transition occurs at a roughly constant magnetic field $B^* \approx 0.65$ T, slightly lower than the critical field of the Al shell, $B_c \approx 0.8$ T [35]. This transition is likely caused by quasiparticle poisoning in the superconducting shell, favored by the suppression of pairing in Al [36]. In region II, B^* decreases gradually with gate voltage, albeit in an irregular fashion. In region III, B^* is constant and equal to a low value $B^* \approx 50$ mT. In Fig. 2(b) we show the field dependence of the peak spacing distribution for each region.

We note that in Fig. 2(a) an even-odd regime, which is present each time the transition from $2e$- to $1e$-periodicity occurs, is likely to be assimilated with the $1e$ regime, because the median does not distinguish a bimodal distribution of spacings from a unimodal one. The even-odd regime is weakly visible in the standard deviation of the peak spacing distribution, which is larger in the low-field $1e$ regime of regions II and III than in the high-field metallic regime of region I [35]. It is also interesting to notice a weak resurgence of $2e$ spacings at $B \approx 0.2$ T in region III. Similar results were obtained on another phase diagram measurement [35].

III. SIMULATIONS OF A PROXIMITIZED NANOWIRE ISLAND

To shed light on the parity phase diagram, we perform numerical simulations of a proximitized InSb island.

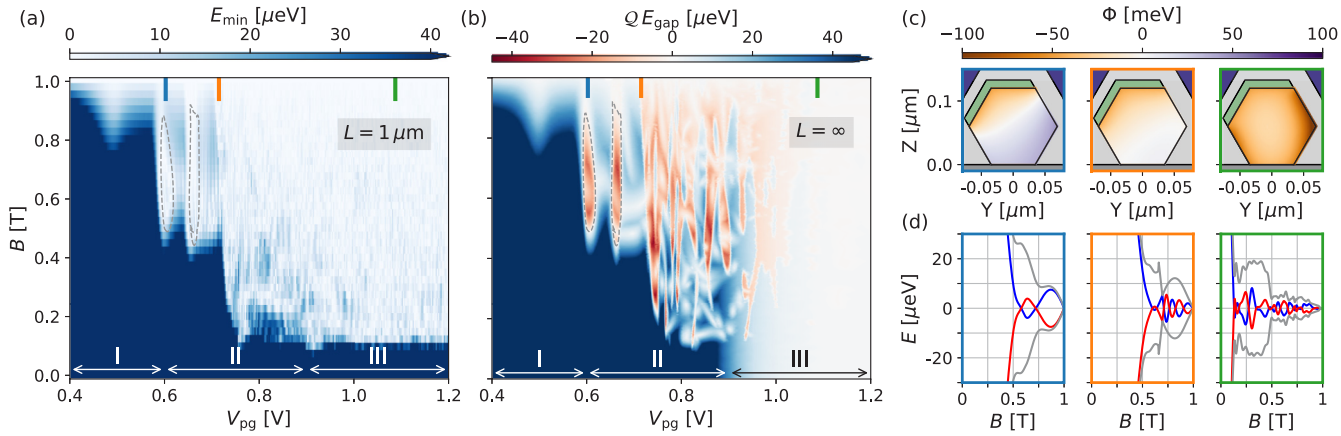

FIG. 3. (a) Quasiparticle energy gap $E_{\min}$ as a function of plunger voltage V_{pg} and magnetic field for the simulated island of length 1 μm. We indicate regimes I, II, and III as in Fig. 2. The energy scale is saturated at 40 μeV because this is the estimated charging energy in the experimental device and thus the expected boundary at which the $2e \to 1e$ transition would start to occur. We note that this boundary is only weakly sensitive to the level of disorder used in the simulations, likely due to the short length of the wire [35]. (b) Bulk topological phase diagram indicating the bulk gap E_{gap} and the sign of the topological index $\mathcal{Q} = \pm 1$, both obtained via the simulation of the band structure of an infinitely long wire. Red regions are topological. Two topological regimes with large gap and small coherence length are marked by the dashed gray lines in both panels (a) and (b). (c) Electrostatic potential profiles in the nanowire cross section for the three plunger gate values indicated by blue, orange, and green bars in panels (a) and (b). (d) Magnetic field dependence of the lowest (red/blue) and first excited (gray) energy levels for three different plunger values. The left panel (blue) crosses a topological region of the phase diagram, while the two other panels (orange and green) correspond to topologically trivial regions.

Advances in the modeling of semiconductor-superconductor hybrid structures allow the inclusion of important effects such as self-consistent electrostatics, orbital magnetic field contribution, and strong coupling between semiconductor and superconductor [37–42]. By integrating out the superconductor into self-energy boundary conditions, we can simulate three-dimensional wires with realistic dimensions including all of the aforementioned effects [17,43]. This approach takes into account the renormalization of semiconductor properties due to the coupling to the superconductor [44].

We model a hexagonal InSb wire with 120 nm facet-to-facet distance and two facets covered by 15 nm Al [Fig. 1(b)]. In Fig. 3(c) we show the simulated electrostatic potential, computed on the level of the Thomas-Fermi approximation [38], inside of the InSb wire for three representative plunger voltages. Since the concentration of fixed charges in the oxide and interface traps at the oxide-semiconductor interface is not known, the charge environment of the device cannot be determined and the plunger gate values will differ in both range and offset between experiment and numerical simulations, and cannot be quantitatively compared. Consistent with the large induced gap observed in InSb-Al devices [34], we assume an electron accumulation layer at the InSb-Al interface [38,39,41,45], with an offset of 50 meV between the interface pinning of the conduction band in InSb and the Fermi energy of Al. This choice is also validated via a numerical comparison with the case of a depletion layer [35]. We cannot exclude the presence of band offset fluctuations in the device, an effect not included in the simulations. The simulations in Fig. 3 are for a clean InSb wire and a critical field $B_c = 1$ T for Al.

In Fig. 3(a) we show the energy gap $E_{\min}$ of an $L = 1$ μm InSb-Al wire, while in Fig. 3(b) we show the bulk energy gap E_{gap} computed from the band structure of an infinitely long wire, with the cross-sectional electrostatic potential chosen to be identical to that which we find in the middle of the 1 μm island. These simulations identify qualitatively the three plunger gate voltage regions of Fig. 2 with different regimes of the proximity effect. The three regimes occur depending on the ratio between the parent superconductor gap Δ_{Al} and the semiconductor-superconductor coupling Γ [46], which depends on the gate voltage [39,41,45].

In region I, $\Gamma \gg \Delta_{Al}$: InSb is strongly proximitized by Al, leading to significant g-factor renormalization such that the induced gap only vanishes when B is close to $B_{c,Al}$. This explains the large experimental value of B^* in this region. The simulations do not include pair-breaking effects in the Al shell, which in reality lead to a regime of gapless superconductivity at B slightly lower than B_c [47]. Region II is a crossover region, $\Gamma \approx \Delta_{Al}$, in which Γ and the strength of induced superconductivity gradually decrease with gate voltage. In region III, Γ vanishes for some semiconductor states due to accumulation away from the Al interface [41], and thus the band structure is gapless already at $B = 0$ [Fig. 3(b)]. In this region, the finite wire is *not* gapless [Fig. 3(a)]: $E_{\min}$ reaches zero only at a small but finite B, similar to what is observed in the experiment.

This surprising feature is a result of finite-size and orbital effects. In the finite length island, scattering due to the inhomogeneous electrostatic potential at the ends of the wire couples unproximitzed modes and proximitized ones, such that all semiconducting states become gapped [48,49]. Thus, in region III the gap at $B = 0$ is finite in Fig. 3(a), but not in the band-structure calculation of Fig. 3(b). However, this gap is fragile: the orbital effect of the magnetic field is strong [40] and leads to the gap closing once half of a flux quantum threads the cross-section area A, so that $B^*_{III} \approx h/(4eA) \approx 0.1$ T [41]. A comparison with a simulation in which orbital effects

are absent [35] confirms that they are crucial to explain the data.

IV. COULOMB OSCILLATIONS IN REGION II

For inducing topological superconductivity with well-separated Majorana zero modes, region III is unsuitable due to the vanishing bulk gap. Region II is more promising: in the infinite length limit, it hosts topological phases with a sizable gap, as indicated by the dashed gray lines in Fig. 3(b). In a finite island, identifying these topological phases is hard due to the energy splitting between Majorana zero modes [30,33], a problem exacerbated by the narrowness of the topological phases in the plunger gate. Numerical simulations indicate that the shortest coherence length achievable in the topological phase is $\approx$200 nm, but it occurs only in small pockets of the phase diagram [35]. Even this optimal value leads to a sizable splitting with characteristic field oscillations of increasing amplitude [Fig. 3(d)]. To complicate the matter further, similar oscillations can also be observed in topologically trivial regions, as also shown in Fig. 3(d). We note that in our simulations the oscillation amplitude increases with field in the topological phase, but not necessarily in the trivial phase [26,30,33].

These energy oscillations can be measured in detail as they reveal themselves in the even-odd peak spacings of conductance oscillations [10]. An example measured in region II is shown in Fig. 4(a). The $2e$-spaced peaks first split at $B \approx 0.3$ T, leading to a brief $2e$ regime with odd valleys [13] and then to an even-odd regime, for which we show peak spacing oscillations in Fig. 4(b). The peak spacings undergo one oscillation in magnetic field before the onset of regularly spaced $1e$ peaks at $B \approx 0.65$ T, likely due to poisoning in the Al shell. The amplitude and position of the peak spacing oscillations change across neighboring valleys, increasing with gate voltage and conferring each valley an individual character [Fig. 4(c)]. This shift could be attributed to the strong gate lever arm causing a change in the effective chemical potential of the proximitized InSb bands.

Together with peak spacing oscillations, we also observe oscillating peak heights [Fig. 4(b)], captured by the asymmetry parameter $\Lambda = G_{e\to o}/(G_{e\to o} + G_{o\to e})$ where $G_{e\to o}$ and $G_{o\to e}$ are two neighboring peak heights [50]. Λ is related to the electron and hole components of the subgap state mediating the transport at the charge degeneracy point. In a minimal theory of two coupled Majorana zero modes, it is predicted to oscillate in antiphase with the energy oscillations [51]. Such a correlation between peak spacing and peak heights is visible in Figs. 4(b) and 4(c): in each valley, the symmetric peak heights ($\Lambda = 0.5$) occurring at $B \approx 0.55$ T have close-to-maximal peak spacings. Other datasets taken in region II show similar behavior [35]. However, in the presence of only a single oscillation we cannot take this as conclusive evidence distinguishing Majorana zero modes from subgap states of trivial origin.

V. CONCLUSIONS

To conclude, our measurements and simulations have brought to light a mechanism behind the $2e$-to-$1e$ transition

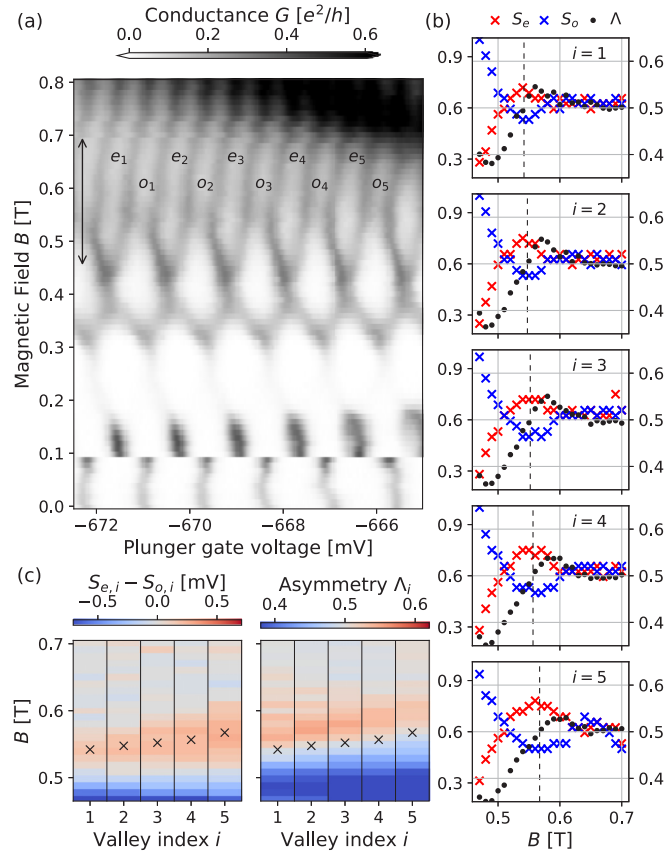

FIG. 4. (a) Coulomb blockade oscillations measured versus plunger gate and magnetic field in region II of the phase diagram. The measurement covers five pairs of even-odd Coulomb valleys (labeled by index $i = 1, \ldots, 5$) in the field range indicated by the black arrow. (b) Field dependence of the even and odd peak spacings $S_{e,o}$ (left y axis, in mV) and of the peak height asymmetry Λ (right y axis) for each pair of Coulomb valleys. Vertical dashed lines denote the linearly interpolated values of B at which $\Lambda = 0.5$, corresponding to equal peak heights. These values of B closely match extremal points in $S_{e,o}$. (c) Peak spacing difference and peak height asymmetry as a function of magnetic field. Black crosses correspond to the values of B denoted by vertical dashed lines in panel (b).

in proximitized nanowires, distinct from the transition into a topological phase. As a consequence, we are able to considerably restrict the range of plunger gate voltage compatible with the presence of Majorana zero-energy modes, although finite-size effects prevent us from a conclusive identification. A strategy to overcome this obstacle is to measure a sequence of parity phase diagrams as in Fig. 2 for wires of increasing length. This would require clean wires to meaningfully compare islands of different length and to preserve the topological phase. Although the mean free path could not be assessed independently in this study, InSb/Al wires have shown convincing signatures of ballistic transport [34]. Finally, given the importance of an extensive search in the parameter space demonstrated in this work, it will be advantageous to speed up the measurement time by adopting faster measurement techniques [52,53].

The raw data and the data analysis code at the basis of the results presented in this work are available online [54].

Additional data as well as more information on methods, numerical simulations with additional results including disorder, and data analysis are available in the Supplemental Material [35].

ACKNOWLEDGMENTS

We acknowledge stimulating discussions with B. Bauer, R. Lutchyn, and T. Laeven. J.S. acknowledges support from National Science Foundation of China under Grant No. 92065203, Chinese Academy of Sciences under Grant No. XDB33000000 and the Synergic Extreme Condition User Facility. This work has been supported by the European Research Council (ERC), the Dutch Organization for Scientific Research (NWO), the Office of Naval Research (ONR), the Laboratory for Physical Sciences, and Microsoft Corporation.

J.S. fabricated the devices with contribution from D.B. in the optimization of the fabrication recipe; S.G., R.L.M.O.H.V., D.C., J.A.L., M.P., C.J.P., and E.P.A.M.B. carried out the growth of materials; J.S. performed the measurements in collaboration with F.B., S.H., and D.vD; J.S., G.W.W., F.B., S.H., V.L., J.-Y.W., L.P.K., and B.vH. discussed and interpreted the experimental data; B.vH. and J.S. implemented the experimental data analysis with input from G.W.W., F.B., and S.H.; G.W.W. ran the numerical simulations and analyzed the simulation results; J.S., G.W.W., F.B., S.H., L.P.K., and B.vH. formulated the comparison between experimental and simulation data; J.S., G.W.W., and B.vH. wrote the paper considering input from all authors.

[1] J. von Delft and D. Ralph, Spectroscopy of discrete energy levels in ultrasmall metallic grains, Phys. Rep. **345**, 61 (2001).

[2] P. Lafarge, P. Joyez, D. Esteve, C. Urbina, and M. H. Devoret, Measurement of the Even-Odd Free-Energy Difference of an Isolated Superconductor, Phys. Rev. Lett. **70**, 994 (1993).

[3] L. J. Geerligs, V. F. Anderegg, J. Romijn, and J. E. Mooij, Single Cooper-Pair Tunneling in Small-Capacitance Junctions, Phys. Rev. Lett. **65**, 377 (1990).

[4] M. T. Tuominen, J. M. Hergenrother, T. S. Tighe, and M. Tinkham, Experimental Evidence for Parity-Based 2*e* Periodicity in a Superconducting Single-Electron Tunneling Transistor, Phys. Rev. Lett. **69**, 1997 (1992).

[5] T. M. Eiles, J. M. Martinis, and M. H. Devoret, Even-Odd Asymmetry of a Superconductor Revealed by the Coulomb Blockade of Andreev Reflection, Phys. Rev. Lett. **70**, 1862 (1993).

[6] A. T. Johnson, L. P. Kouwenhoven, W. de Jong, N. C. van der Vaart, C. J. P. M. Harmans, and C. T. Foxon, Zero-Dimensional States and Single Electron Charging in Quantum Dots, Phys. Rev. Lett. **69**, 1592 (1992).

[7] E. B. Foxman, P. L. McEuen, U. Meirav, N. S. Wingreen, Y. Meir, P. A. Belk, N. R. Belk, M. A. Kastner, and S. J. Wind, Effects of quantum levels on transport through a Coulomb island, Phys. Rev. B **47**, 10020 (1993).

[8] Y. Alhassid, The statistical theory of quantum dots, Rev. Mod. Phys. **72**, 895 (2000).

[9] A. P. Higginbotham, S. M. Albrecht, G. Kiršanskas, W. Chang, F. Kuemmeth, P. Krogstrup, T. S. Jespersen, J. Nygård, K. Flensberg, and C. M. Marcus, Parity lifetime of bound states in a proximitized semiconductor nanowire, Nat. Phys. **11**, 1017 (2015).

[10] S. M. Albrecht, A. P. Higginbotham, M. Madsen, F. Kuemmeth, T. S. Jespersen, J. Nygård, P. Krogstrup, and C. M. Marcus, Exponential protection of zero modes in Majorana islands, Nature (London) **531**, 206 (2016).

[11] S. M. Albrecht, E. B. Hansen, A. P. Higginbotham, F. Kuemmeth, T. S. Jespersen, J. Nygård, P. Krogstrup, J. Danon, K. Flensberg, and C. M. Marcus, Transport Signatures of Quasiparticle Poisoning in a Majorana Island, Phys. Rev. Lett. **118**, 137701 (2017).

[12] E. C. T. O'Farrell, A. C. C. Drachmann, M. Hell, A. Fornieri, A. M. Whiticar, E. B. Hansen, S. Gronin, G. C. Gardner, C. Thomas, M. J. Manfra, K. Flensberg, C. M. Marcus, and F. Nichele, Hybridization of Subgap States in One-Dimensional Superconductor-Semiconductor Coulomb Islands, Phys. Rev. Lett. **121**, 256803 (2018).

[13] J. Shen, S. Heedt, F. Borsoi, B. van Heck, S. Gazibegovic, R. L. M. Op het Veld, D. Car, J. A. Logan, M. Pendharkar, S. J. L. Ramakers, G. Wang, D. Xu, D. Bouman, A. Geresdi, C. J. Palmstrøm, E. P. A. M. Bakkers, and L. P. Kouwenhoven, Parity transitions in the superconducting ground state of hybrid InSb–Al Coulomb islands, Nat. Commun. **9**, 1 (2018).

[14] S. Vaitiekėnas, A. M. Whiticar, M.-T. Deng, F. Krizek, J. E. Sestoft, C. J. Palmstrøm, S. Marti-Sanchez, J. Arbiol, P. Krogstrup, L. Casparis, and C. M. Marcus, Selective-Area-Grown Semiconductor-Superconductor Hybrids: A Basis for Topological Networks, Phys. Rev. Lett. **121**, 147701 (2018).

[15] J. van Veen, A. Proutski, T. Karzig, D. I. Pikulin, R. M. Lutchyn, J. Nygård, P. Krogstrup, A. Geresdi, L. P. Kouwenhoven, and J. D. Watson, Magnetic-field-dependent quasiparticle dynamics of nanowire single-Cooper-pair transistors, Phys. Rev. B **98**, 174502 (2018).

[16] M. Pendharkar, B. Zhang, H. Wu, A. Zarassi, P. Zhang, C. P. Dempsey, J. S. Lee, S. D. Harrington, G. Badawy, S. Gazibegovic, J. Jung, A. H. Chen, M. A. Verheijen, M. Hocevar, E. P. A. M. Bakkers, C. J. Palmstrøm, and S. M. Frolov, Parity-preserving and magnetic field-resilient superconductivity in InSb nanowires with Sn shells, Science **372**, 508 (2021).

[17] S. Vaitiekenas, G. W. Winkler, B. van Heck, T. Karzig, M.-T. Deng, K. Flensberg, L. I. Glazman, C. Nayak, P. Krogstrup, R. M. Lutchyn, and C. M. Marcus, Flux-induced topological superconductivity in full-shell nanowires, Science **367**, eaav3392 (2020).

[18] A. M. Whiticar, A. Fornieri, E. C. T. O'Farrell, A. C. C. Drachmann, T. Wang, C. Thomas, S. Gronin, R. Kallaher, G. C. Gardner, M. J. Manfra, C. M. Marcus, and F. Nichele, Coherent transport through a Majorana island in an Aharonov–Bohm interferometer, Nat. Commun. **11**, 1 (2020).

[19] D. J. Carrad, M. Bjergfelt, T. Kanne, M. Aagesen, F. Krizek, E. M. Fiordaliso, E. Johnson, J. Nygård, and T. S.

Jespersen, Shadow epitaxy for in situ growth of generic semiconductor/superconductor hybrids, Adv. Mater. **32**, 1908411 (2020).

[20] T. Kanne, M. Marnauza, D. Olsteins, D. J. Carrad, J. E. Sestoft, J. de Bruijckere, L. Zeng, E. Johnson, E. Olsson, K. Grove-Rasmussen, and J. Nygård, Epitaxial Pb on InAs nanowires for quantum devices, Nat. Nanotechnol. **16**, 776 (2021).

[21] R. M. Lutchyn, E. P. A. M. Bakkers, L. P. Kouwenhoven, P. Krogstrup, C. M. Marcus, and Y. Oreg, Majorana zero modes in superconductor–semiconductor heterostructures, Nat. Rev. Mater. **3**, 52 (2018).

[22] L. Fu, Electron Teleportation via Majorana Bound States in a Mesoscopic Superconductor, Phys. Rev. Lett. **104**, 056402 (2010).

[23] B. van Heck, R. M. Lutchyn, and L. I. Glazman, Conductance of a proximitized nanowire in the Coulomb blockade regime, Phys. Rev. B **93**, 235431 (2016).

[24] C. Nayak, S. H. Simon, A. Stern, M. Freedman, and S. Das Sarma, Non-Abelian anyons and topological quantum computation, Rev. Mod. Phys. **80**, 1083 (2008).

[25] T. Karzig, C. Knapp, R. M. Lutchyn, P. Bonderson, M. B. Hastings, C. Nayak, J. Alicea, K. Flensberg, S. Plugge, Y. Oreg, C. M. Marcus, and M. H. Freedman, Scalable designs for quasiparticle-poisoning-protected topological quantum computation with Majorana zero modes, Phys. Rev. B **95**, 235305 (2017).

[26] C.-K. Chiu, J. D. Sau, and S. Das Sarma, Conductance of a superconducting Coulomb-blockaded Majorana nanowire, Phys. Rev. B **96**, 054504 (2017).

[27] E. J. H. Lee, X. Jiang, M. Houzet, R. Aguado, C. M. Lieber, and S. De Franceschi, Spin-resolved Andreev levels and parity crossings in hybrid superconductor–semiconductor nanostructures, Nat. Nanotechnol. **9**, 79 (2014).

[28] J. Chen, B. D. Woods, P. Yu, M. Hocevar, D. Car, S. R. Plissard, E. P. A. M. Bakkers, T. D. Stanescu, and S. M. Frolov, Ubiquitous Non-Majorana Zero-Bias Conductance Peaks in Nanowire Devices, Phys. Rev. Lett. **123**, 107703 (2019).

[29] E. Prada, P. San-Jose, M. W. A. de Moor, A. Geresdi, E. J. H. Lee, J. Klinovaja, D. Loss, J. Nygård, R. Aguado, and L. P. Kouwenhoven, From Andreev to Majorana bound states in hybrid superconductor–semiconductor nanowires, Nat. Rev. Phys. **2**, 575 (2020).

[30] S. Das Sarma, J. D. Sau, and T. D. Stanescu, Splitting of the zero-bias conductance peak as smoking gun evidence for the existence of the Majorana mode in a superconductor-semiconductor nanowire, Phys. Rev. B **86**, 220506(R) (2012).

[31] O. Dmytruk and J. Klinovaja, Suppression of the overlap between Majorana fermions by orbital magnetic effects in semiconducting-superconducting nanowires, Phys. Rev. B **97**, 155409 (2018).

[32] Z. Cao, H. Zhang, H.-F. Lü, W.-X. He, H.-Z. Lu, and X. C. Xie, Decays of Majorana or Andreev Oscillations Induced by Steplike Spin-Orbit Coupling, Phys. Rev. Lett. **122**, 147701 (2019).

[33] G. Sharma, C. Zeng, T. D. Stanescu, and S. Tewari, Hybridization energy oscillations of Majorana and Andreev bound states in semiconductor-superconductor nanowire heterostructures, Phys. Rev. B **101**, 245405 (2020).

[34] S. Gazibegovic, D. Car, H. Zhang, S. C. Balk, J. A. Logan, M. W. A. de Moor, M. C. Cassidy, R. Schmits, D. Xu, G. Wang *et al.*, Epitaxy of advanced nanowire quantum devices, Nature (London) **548**, 434 (2017).

[35] See Supplemental Material at http://link.aps.org/supplemental/10.1103/PhysRevB.104.045422 for additional datasets, numerical simulations and information on the data analysis.

[36] M. T. Tuominen, J. M. Hergenrother, T. S. Tighe, and M. Tinkham, Even-odd electron number effects in a small superconducting island: Magnetic-field dependence, Phys. Rev. B **47**, 11599 (1993).

[37] A. Vuik, D. Eeltink, A. R. Akhmerov, and M. Wimmer, Effects of the electrostatic environment on the Majorana nanowire devices, New J. Phys. **18**, 033013 (2016).

[38] A. E. G. Mikkelsen, P. Kotetes, P. Krogstrup, and K. Flensberg, Hybridization at Superconductor-Semiconductor Interfaces, Phys. Rev. X **8**, 031040 (2018).

[39] A. E. Antipov, A. Bargerbos, G. W. Winkler, B. Bauer, E. Rossi, and R. M. Lutchyn, Effects of Gate-Induced Electric Fields on Semiconductor Majorana Nanowires, Phys. Rev. X **8**, 031041 (2018).

[40] G. W. Winkler, D. Varjas, R. Skolasinski, A. A. Soluyanov, M. Troyer, and M. Wimmer, Orbital Contributions to the Electron g Factor in Semiconductor Nanowires, Phys. Rev. Lett. **119**, 037701 (2017).

[41] G. W. Winkler, A. E. Antipov, B. van Heck, A. A. Soluyanov, L. I. Glazman, M. Wimmer, and R. M. Lutchyn, Unified numerical approach to topological semiconductor-superconductor heterostructures, Phys. Rev. B **99**, 245408 (2019).

[42] B. Nijholt and A. R. Akhmerov, Orbital effect of magnetic field on the Majorana phase diagram, Phys. Rev. B **93**, 235434 (2016).

[43] A. Kringhøj, G. W. Winkler, T. W. Larsen, D. Sabonis, O. Erlandsson, P. Krogstrup, B. van Heck, K. D. Petersson, and C. M. Marcus, Andreev Modes from Phase Winding in a Full-Shell Nanowire-Based Transmon, Phys. Rev. Lett. **126**, 047701 (2021).

[44] W. S. Cole, S. Das Sarma, and T. D. Stanescu, Effects of large induced superconducting gap on semiconductor Majorana nanowires, Phys. Rev. B **92**, 174511 (2015).

[45] M. W. A. de Moor, J. D. S. Bommer, D. Xu, G. W. Winkler, A. E. Antipov, A. Bargerbos, G. Wang, N. Van Loo, R. L. M. Op het Veld, S. Gazibegovic *et al.*, Electric field tunable superconductor-semiconductor coupling in Majorana nanowires, New J. Phys. **20**, 103049 (2018).

[46] T. D. Stanescu, R. M. Lutchyn, and S. Das Sarma, Majorana fermions in semiconductor nanowires, Phys. Rev. B **84**, 144522 (2011).

[47] A. I. Larkin, Superconductor of small dimensions in a strong magnetic field, J. Exptl. Theoret. Phys. (U.S.S.R.) **48**, 232 (1965) [Sov. Phys. JETP **21**, 153 (1965)].

[48] A. Haim and A. Stern, Benefits of Weak Disorder in One-Dimensional Topological Superconductors, Phys. Rev. Lett. **122**, 126801 (2019).

[49] T. Laeven, B. Nijholt, M. Wimmer, and A. R. Akhmerov, Enhanced Proximity Effect in Zigzag-Shaped Majorana Josephson Junctions, Phys. Rev. Lett. **125**, 086802 (2020).

[50] In Figs. 4(b) and 4(c) we plot the average value over two neighboring o $\rightarrow$ e peaks for each even valley.

[51] E. B. Hansen, J. Danon, and K. Flensberg, Probing electron-hole components of subgap states in Coulomb blockaded Majorana islands, Phys. Rev. B **97**, 041411(R) (2018).

[52] M.-C. Harabula, T. Hasler, G. Fülöp, M. Jung, V. Ranjan, and C. Schönenberger, Measuring a quantum dot with an impedance-matching on-chip superconducting *LC* resonator at gigahertz frequencies, Phys. Rev. Appl. **8**, 054006 (2017).

[53] D. Razmadze, D. Sabonis, F. K. Malinowski, G. C. Ménard, S. Pauka, H. Nguyen, D. M. T. van Zanten, E. C. T. O'Farrell, J. Suter, P. Krogstrup, F. Kuemmeth, and C. M. Marcus, Radio-Frequency Methods for Majorana-Based Quantum Devices: Fast Charge Sensing and Phase-Diagram Mapping, Phys. Rev. Appl. **11**, 064011 (2019).

[54] J. Shen, G. W. Winkler, F. Borsoi, S. Heedt, V. Levajac, J.-Y. Wang, D. van Driel, D. Bouman, S. Gazibegovic, R. L. M. op het Veld, D. Car, J. A. Logan, M. Pendharkar, C. J. Palmstrom, E. P. A. M. Bakkers, L. P. Kouwenhoven, and B. van Heck, "A full parity phase diagram of a proximitized nanowire island: Data and Code", doi: 10.4121/13333451.v4 (2021).